*Int. J. Multiphase Flow*, Vol. 3, pp. 147–169. Pergamon/Elsevier, 1976. Printed in Great Britain.

# STOKES FLOW PAST FINITE COAXIAL CLUSTERS OF SPHERES IN A CIRCULAR CYLINDER

S. LEICHTBERG,† R. PFEFFER and S. WEINBAUM
The City College of the City University of New York, U.S.A.

(*Received* 21 *July* 1975. *In revised form* 4 *March* 1976)

**Abstract**—Solutions are presented for the Stokes flow past finite axial assemblages of up to 9 spheres in an infinitely long cylindrical tube for a wide range of sphere spacings and sphere to cylinder diameter ratios. General solutions are constructed from the fundamental solutions to the governing equation in both the cylindrical and spherical coordinate systems. No-slip boundary conditions are enforced on the tube surface by constructing the Fourier transform of the general disturbance created by the spheres, as detected on the cylinder wall. The boundary conditions are then applied on the sphere surfaces by a previously developed series truncation technique.

The calculated drag forces and zero-drag velocities demonstrate the interparticle interaction effects, the sphere-wall interactions, and the effects of wall damping on the inter-particle shielding phenomenon.

## 1. INTRODUCTION

The slow motion of an incompressible viscous fluid relative to assemblages of submerged particles has long been of interest in the areas of sedimentation, flow through packed and fluidized beds, suspension velocities, pollution abatement, and other engineering and bio–engineering applications.

One particularly intriguing application is a study of the transient phenomenon of the formation of aggregates of red blood cells, or rouleaux, in the microcapillaries. It has been demonstrated by Leichtberg *et al.* (1976*a*) and Leichtberg *et al.* (1976*b*) that the unequal particle interaction forces between identical red cells, which continually change as a function of particle spacing and velocity, provide a new hydrodynamic mechanism for the possible formation of rouleaux. These papers, however, deal exclusively with transient flows in unbounded and quasi-bounded media. This paper provides the necessary logical link by establishing the limits of validity of extrapolating the results of unbounded flow theory to the bounded flow reality of the microcirculation. It is shown here that the interparticle interactions observed in the unbounded flow problem also exist when the flow is bounded, but are subjected to wall damping which becomes significant at particle-to-tube diameter ratios of 0.5 or greater.

The problem considered in this paper is the flow past a finite chain of rigid spheres moving slowly in a viscous fluid, which may be moving or stationary, inside an infinitely long cylindrical tube. The problems of multi-particle slow viscous flow have been previously treated extensively by four major approaches—the method of reflections, the point force approximation, the finite element method, and the technique of internal singularity distributions.

The method of reflections, developed by Smoluchowski (1911, 1912) and used by Burgers (1940), Kynch (1959), and Happel & Brenner (1965) is an iterative approximation technique which has been extensively used to solve multi-particle and particle–wall interaction problems. Bohlin (1960), using an extension of the method of reflections as originally presented by Faxen (1923), obtained drag results for a single sphere moving along the axis of a cylinder which exhibit very good agreement with the earlier, more exact solution of Haberman & Sayre (1958), for sphere-to-cylinder diameter ratios of up to 0.6. For higher diameter ratios Bohlin's method breaks down due to certain simplifying assumptions. Other investigations using the method of reflections were conducted by Ladenburg (1907) and Faxen (1922) who studied the drag on spheres moving in a still liquid inside a long cylindrical tube. Wakiya (1953) and Happel & Byrne (1954) have examined a single sphere in Poiseuille flow inside a long cylinder, and Greenstein & Happel (1970) studied the

†Present address: Pratt & Whitney Aircraft, East Hartford, CT, U.S.A.

axial motion of two spheres perpendicular to their line of centers, obtaining results which are in excellent agreement with the experimental results of Bart (1959).

The convergence characteristics of the method of reflections are strongly dependent on the ratio of the particle dimensions to the spacing between the particles and/or wall. When this ratio is small (i.e. a dilute system), a single reflection describes the particle interaction adequately, as was done by Hocking (1964). For concentrated systems (the ratio approaching unity) higher order interaction effects become significant. The leading term in the iterative series solution becomes a poor description of particle interaction effects and generates a series with very slow convergence characteristics. Furthermore, this method is extremely tedious to apply when more than two particles are present and thus would be very inefficient for treating the bounded finite particle assemblages considered in the present study.

The point force technique, developed by Burgers (1938, 1941, 1942) and used by others, is only a useful approximation for dilute systems. It is inapplicable to concentrated systems or to any bounded flow, because of the inability of point forces to account for the angular dependence of disturbance on one surface due to the presence of other boundaries.

The finite-element treatment of multi-particle slow flow was recently used by Skalak *et al.* (1972) in a capillary blood flow application. This method is a very promising technique for irregular but identical particles with periodic spacing. The method cannot easily be applied to transient interaction problems where the particle boundary conditions are not periodic, because of the slow decay properties of Stokes flow disturbances.

The techniques described above have not been used when more than two objects are present except for the special case of the flow relative to an infinite chain of equally spaced particles along their line of centers. Because of the perfect periodicity existing in such infinite chains, this latter problem can be viewed as the flow past a single particle in a cell with periodic boundary conditions, e.g. Wang & Skalak (1969) and Chen & Skalak (1970).

The technique of describing solid boundaries by a distribution of internal singularities is based on the work of Payne & Pell (1960) who have shown that the infinite set of simply separable singular solutions for each co-ordinate system provides a complete set of generating functions, which can be used to satisfy rather general viscous flow boundary conditions along any constant co-ordinate surface of the same orthogonal co-ordinate system. Gluckman *et al.* (1971) have taken advantage of the completeness of these fundamental separable solutions to obtain the exact Stokes solutions for a finite line array of spheres or spheroids in unbounded media, by placing a single infinite sequence of appropriate singularities at the origin of each sphere or spheroid. This study has shown that it is most efficient to use a truncated series of point singularities, and satisfy boundary conditions at discrete points on each object simultaneously. This method, the multipole truncation technique, yields first-, second-, and fifth-order truncation solutions for the drag which are accurate to 2.5, 0.1, and 0.001% respectively, for flow parallel to the axis of two touching spheres, in sharp contrast to the poor results obtained by the method of reflections. This method was later extended in Gluckman *et al.* (1972) to the exact treatment of axisymmetric Stokes flow past an arbitrary convex body of revolution in an unbounded medium.

The principles developed by Payne & Pell were also used by Haberman & Sayre (1958) in obtaining an "exact" solution for a single sphere moving along the axis of an infinitely long cylinder. They employed the general solutions of the creeping motion equations in both the cylindrical and spherical co-ordinate systems, the latter being an expansion of the stream function. Wall correction factors were obtained for both rigid and fluid spheres, in both moving and stationary media.

Hochmuth & Sutera (1970) treated the motion of a large sphere moving concentrically inside a long tube by combining the methods of Haberman & Sayre (1958) with lubrication theory arguments. The problem of a small sphere eccentrically located in close proximity to a tube wall was treated by Bungay & Brenner (1973*a*) via a regular perturbation procedure. Bungay & Brenner (1973*b*) employ a singular perturbation technique to examine asymmetric situations in which the

sphere occupies virtually the entire cross-section of the cylinder. Brenner (1970, 1971) studied the motion of a small, eccentric, neutrally-buoyant solid particle or liquid droplet, demonstrating that the pressure drop could be obtained without the need for a detailed solution satisfying the boundary conditions on the tube wall.

The technique used in the present paper for finite chains of spheres inside a cylinder utilizes the infinite set of simply separable singular solutions in both the spherical and cylindrical coordinate systems to satisfy the tube boundary conditions, by constructing the Fourier transform of the spherical disturbances. The resulting solution satisfies the boundary conditions on the cylinder identically and is then used to satisfy the boundary conditions on all the spheres simultaneously in a manner similar to the multipole truncation technique developed in Gluckman *et al.* (1971).

Section 2 presents the formulation of the problem, its governing equations and the boundary conditions. Section 3 outlines the solution procedure, and section 4 deals with the methods of calculating either the drag forces or zero-drag velocities. Sections 5 and 6 then present and discuss the results.

## 2. FORMULATION OF THE PROBLEM

The flows considered in this paper are assumed to be axisymmetric (see figure 1), so that the Stokes stream function exists. It is further assumed that the motion is sufficiently slow for the creeping motion equations to be valid:

$$\nabla p = \mu \nabla^2 \mathbf{V}, \tag{2.1}$$

$$\nabla \cdot \mathbf{V} = 0. \tag{2.2}$$

Taking the curl of both sides of [2.1] and introducing [2.2] and the stream function results in a fourth-order linear partial differential equation for the stream function:

$$\boldsymbol{\omega} = \nabla \times \mathbf{V} = \mathbf{i}_3 h_3 E^2 \psi, \tag{2.3}$$

$$E^2(E^2\psi) = 0, \tag{2.4}$$

where

$$E^2 = \frac{h_1 h_2}{h_3}\left[\frac{\partial}{\partial q_1}\left(\frac{h_1 h_3}{h_2}\frac{\partial}{\partial q_1}\right) + \frac{\partial}{\partial q_2}\left(\frac{h_2 h_3}{h_1}\frac{\partial}{\partial q_2}\right)\right]. \tag{2.5}$$

Here $(q_1, q_2, q_3)$ are generalized orthogonal curvilinear coordinates, $h_1$, $h_2$, $h_3$ are the metrical coefficients of this coordinate system, $E^2$ is the generalized axisymmetric Stokesian linear operator, $\boldsymbol{\omega}$ is the vorticity, and $\psi = \psi(q_1, q_2)$ is the Stokes stream function. In cylindrical coordinates, [2.5] reduces to (see figure 1 for coordinate definition)

$$E^2 = \frac{\partial^2}{\partial R^2} - \frac{1}{R}\frac{\partial}{\partial R} + \frac{\partial^2}{\partial z^2}, \tag{2.6}$$

and in spherical coordinates,

$$E^2 = \frac{\partial^2}{\partial r^2} + \frac{1-\zeta^2}{r^2}\frac{\partial^2}{\partial \zeta^2}, \tag{2.7}$$

where

$$\zeta = \cos\theta, \tag{2.8}$$

$$E^2\psi = \omega r \sin\theta = R\omega. \tag{2.9}$$

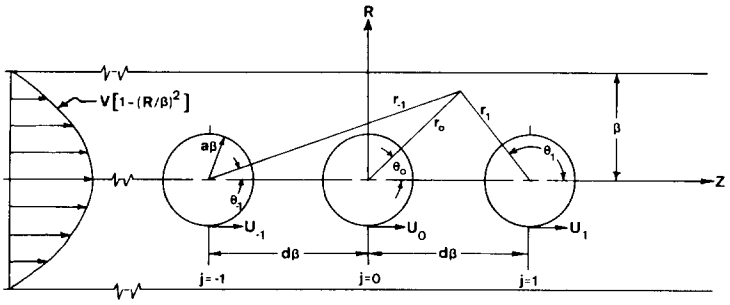


Figure 1. The system geometry.

The geometry being considered is shown in figure 1. The various spheres in the $N$-sphere chain are equally spaced and are indexed from $-(N-1)/2$ to $(N-1)/2$ with the origin taken at the central sphere for convenience. Accordingly, the system is symmetrical about the $z = 0$ plane, and the descriptive equations are expected to be even functions of $z$ if the sphere velocities $U_j$ pattern the same symmetry. For an even number of spheres, a slight rearrangement achieves the same result. The far downstream flow is Poiseuillian,

$$v(R) = V\left(1 - \frac{R^2}{\beta^2}\right), \tag{2.10}$$

where $V$ is the downstream centerline velocity and is related to the discharge, $Q$, by

$$Q = \frac{\pi}{2}\beta^2 V. \tag{2.11}$$

From [2.10] the stream function at plus and minus infinity is given by

$$\psi = V\beta^2\left[\frac{1}{2}\left(\frac{R}{\beta}\right)^2 - \frac{1}{4}\left(\frac{R}{\beta}\right)^4\right], \quad |z| \to \infty, \tag{2.12}$$

The no-slip boundary condition on the cylinder wall, $R = \beta$, is

$$\left.\begin{aligned} v_z &= 0 \qquad (2.13a)\\ \psi &= \frac{1}{4}V\beta^2 \qquad (2.13b)\end{aligned}\right\} R = \beta.$$

On each of the $N$ sphere surfaces, $r_j = a\beta$, the boundary conditions are

$$\left.\begin{aligned} v_z &= U_j \quad \text{on} \quad r_j = a\beta \qquad (2.14a)\\ v_R &= 0 \qquad j = -\frac{N-1}{2} \ \text{to} \ \frac{N-1}{2}. \qquad (2.14b)\end{aligned}\right\}$$

## 3. SOLUTION

The general solutions to $E^4\psi = 0$ are originally due to Sampson (1891), but are also given by Savic (1953) and Haberman & Sayre (1958). In the cylindrical-coordinate system $(R, z)$, the general solution, which is symmetric about $z = 0$ and generates finite velocities at $R = 0$ and as $|z| \to \infty$, is

$$\psi(R, z) = a_1R^2 + a_2R^4 + \int_0^\infty [A(t)RI_1(Rt) + B(t)R^2I_0(Rt)]\cos(zt)\,dt, \tag{3.1}$$

where $A(t)$ and $B(t)$ are unknown functions of $t$, $a_1$ and $a_2$ are unknown constants, and $I_0$ and $I_1$ are modified Bessel functions of the first kind. The treatment of geometries which are asymmetrical about $z = 0$ would require the addition of a Fourier sine integral to the solution [3.1], with the subsequent analysis proceeding along parallel lines.

In the spherical coordinate system $(r, \theta)$, the general solution to $E^4\psi = 0$, constrained to vanish on the centerline, and to generate finite velocities on the cylinder axis ($\theta = 0, \pi$) and vanishing disturbances far downstream ($r \to |z| \to \infty$), is

$$\psi(r, \theta) = \sum_{n=2}^{\infty} [C_n r^{-n+1} + D_n r^{-n+3}] \mathcal{T}_n(\zeta), \qquad [3.2]$$

where $\mathcal{T}_n(\zeta)$ are Gegenbauer (ultraspherical) functions of order $n$ and degree 1/2, and $C_n$ and $D_n$ are arbitrary constants of integration.

Equation [3.2], representing a spherical disturbance in the flow field, is singular at the origin of coordinates, $r = 0$. In order to successfully satisfy the no-slip boundary conditions on the surface of each of the $N$ spheres in the chain, it becomes necessary to place the singularity [3.2] at the center of each sphere. Utilizing the linearity of the governing equation and superposing the solutions [3.2] as written from $N$ different origins of coordinates, we construct the spherical solution representing flow field disturbances created by $N$ spheres,

$$\psi = \sum_{j=-(1/2)(N-1)}^{(1/2)(N-1)} \sum_{n=2}^{\infty} [C_{nj} r_j^{-n+1} + D_{nj} r_j^{-n+3}] \mathcal{T}_n(\zeta_j), \quad N = \text{odd}. \qquad [3.3]$$

Here the $r_j$ and $\theta_j$ coordinates are measured from the origin of each sphere considered separately (see figure 1). For $N$ even the origin is taken midway between the two central spheres and the indexing of $j$ is altered.

Equation [3.3] represents a sufficiently general solution to [2.4] for treating the axisymmetric motion of spheres in an unbounded medium (see Gluckman *et al.* 1971). In the present problem, however, the complete solution must also include the cylindrical-coordinate solution [3.1] in order to be able to satisfy the tube conditions as well. Hence, the general solution to [2.4] is constructed as the superposition of the cylindrical solution [3.1] and the spherical disturbance representation [3.3]; i.e.

$$\psi = a_1 R^2 + a_2 R^4 + \int_0^{\infty} [A(t) R I_1(Rt) + B(t) R^2 I_0(Rt)] \cos(zt)\, dt$$
$$+ \sum_j \sum_{n=2}^{\infty} [C_{nj} r_j^{-n+1} + D_{nj} r_j^{-n+3}] \mathcal{T}_n(\zeta_j). \qquad [3.4]$$

The index limits on the outer summation have been omitted for the sake of brevity and generality of application to odd and even-numbered chains, and henceforth it remains understood that the $j$-summation is carried for all the $N$ spheres. As $|z| \to \infty$, [3.4] reduces to

$$[\psi]_{|z| \to \infty} = a_1 R^2 + a_2 R^4.$$

Therefore, requiring a return to Poiseuille flow at infinity, one finds from [2.12] that the constants $a_1$ and $a_2$ are

$$a_1 = \frac{1}{2} V, \quad a_2 = -\frac{1}{4} V \beta^{-2}, \qquad [3.5]$$

and [3.4] becomes

$$\psi = V\beta^2 \left[ \frac{1}{2} \left( \frac{R}{\beta} \right)^2 - \frac{1}{4} \left( \frac{R}{\beta} \right)^4 \right] + \int_0^{\infty} [A(t) R I_1(Rt) + B(t) R^2 I_0(Rt)] \cos(zt)\, dt$$
$$+ \sum_j \sum_{n=2}^{\infty} [C_{nj} r_j^{-n+1} + D_{nj} r_j^{-n+3}] \mathcal{T}_n(\zeta_j). \qquad [3.6]$$

*The cylinder boundary conditions*

Using the properties of Gegenbauer and Legendre functions along with the appropriate transformations between the cylindrical coordinate system $(R, z)$ and the spherical-coordinate systems $(r_j, \theta_j$; all $j)$, the general solution for the stream function [3.6] is differentiated to yield the $z$ and $R$ velocity components:

$$v_z = \frac{1}{R}\frac{\partial \psi}{\partial R} = V\left(1 - \frac{R^2}{\beta^2}\right) + \int_0^\infty \{A(t)tI_0(Rt) + B(t)[RtI_1(Rt) + 2I_0(Rt)]\} \cos(zt)\, dt + \sum_j \sum_{n=2}^{\infty} \{C_{nj}P_n(\zeta_j)r_j^{-n-1} + D_{nj}[P_n(\zeta_j) + 2\mathcal{T}_n(\zeta_j)]r_j^{-n+1}\}, \quad [3.7]$$

$$v_R = -\frac{1}{R}\frac{\partial \psi}{\partial z} = \int_0^\infty [A(t)I_1(Rt) + B(t)RI_0(Rt)]t \sin(zt)\, dt + \sum_j \sum_{n=2}^{\infty} \left\{ C_{nj}\left[\frac{(n+1)\mathcal{T}_{n+1}(\zeta_j)}{\sin\theta_j}\right] r_j^{-n-1} + D_{nj}\left[\frac{(n+1)\mathcal{T}_{n+1}(\zeta_j) - 2\zeta_j(\mathcal{T}_n(\zeta_j))}{\sin\theta_j}\right] r_j^{-n+1} \right\}, \quad [3.8]$$

where $P_n(\zeta_j)$ are Legendre functions.

The tube boundary conditions [2.13] and spherical-to-cylindrical coordinate transformations are then applied to [3.6] and [3.7]. The following two equations result from [2.13a] and [3.7],

$$\int_0^\infty \left\{A(t)tI_0(\beta t) + B(t)[\beta tI_1(\beta t) + 2I_0(\beta t)] \cos(zt)\, dt = -\sum_j \sum_{n=2}^{\infty} [C_{nj}F_n^{(1)}(z_j) + D_{nj}F_n^{(2)}(z_j)]\right\}, \quad [3.9]$$

and from [2.13b] and [3.6],

$$\int_0^\infty [A(t)\beta I_1(\beta t) + B(t)\beta^2 I_0(\beta t)] \cos(zt)\, dt = -\sum_j \sum_{n=2}^{\infty} [C_{nj}F_n^{(3)}(z_j) + D_{nj}F_n^{(4)}(z_j)], \quad [3.10]$$

where, for brevity,

$$z_j \equiv z - jd\beta, \quad [3.11]$$

and

$$F_n^{(1)}(z_j) = (\beta^2 + z_j^2)^{-(n+1)/2} P_n\left[\frac{z_j}{\sqrt{(\beta^2 + z_j^2)}}\right], \quad [3.12a]$$

$$F_n^{(2)}(z_j) = (\beta^2 + z_j^2)^{-n(n-1)/2}\left\{P_n\left[\frac{z_j}{\sqrt{(\beta^2 + z_j^2)}}\right] + 2\mathcal{T}_n\left[\frac{z_j}{\sqrt{(\beta^2 + z_j^2)}}\right]\right\}, \quad [3.12b]$$

$$F_n^{(3)}(z_j) = (\beta^2 + z_j^2)^{-(n-1)/2}\mathcal{T}_n\left[\frac{z_j}{\sqrt{(\beta^2 + z_j^2)}}\right], \quad [3.12c]$$

$$F_n^{(4)}(z_j) = (\beta^2 + z_j^2)^{-(n-3)/2}\mathcal{T}_n\left[\frac{z_j}{\sqrt{(\beta^2 + z_j^2)}}\right]. \quad [3.12d]$$

The right hand sides of [3.9] and [3.10] are representative, to within the yet-unknown $C_{nj}$ and $D_{nj}$ coefficients, of the effect of the spherical disturbances on the cylinder wall, where they are functions of the $z$ coordinate only. Although the individual $F_n^{(k)}(z_j)$ functions $(k = 1, 2, 3, 4)$ are even in $z_j$ for even $n$ and are odd in $z_j$ for odd $n$, the complete right hand side of [3.9] and [3.10] must be

even functions of $z$, since they represent Stokes flow disturbances created by system having geometrical symmetry about $z = 0$.

The left hand sides of [3.9] and [3.10] are seen as Fourier cosine integral representations of their right hand sides. They may be inverted and the resulting equations manipulated somewhat, while keeping in mind the discussion of the previous paragraph. From [3.9] and [3.10], respectively,

$$A(t)tI_0(\beta t) + B(t)[\beta tI_1(\beta t) + 2I_0(\beta t)] = -\sum_j \sum_{n=2}^{\infty} [C_{nj}G_{nj}^{(1)}(t) + D_{nj}G_{nj}^{(2)}(t)], \quad [3.13]$$

$$A(t)\beta I_1(\beta t) + B(t)\beta^2 I_0(\beta t) = -\sum_j \sum_{n=2}^{\infty} [C_{nj}G_{nj}^{(3)}(t) + D_{nj}G_{nj}^{(4)}(t)], \quad [3.14]$$

where, for $k = 1, 2, 3, 4$,

$$G_{nj}^{(k)}(t) = \frac{1}{\pi}\int_{-\infty}^{\infty} F_n^{(k)}(z_j)\cos(zt)\,dz$$

$$= \begin{cases} \dfrac{2}{\pi}\cos(jd\beta t)\displaystyle\int_0^{\infty} F_n^{(k)}(z_j)\cos(z_j t)\,dz_j, & n \text{ even} \\ -\dfrac{2}{\pi}\sin(jd\beta t)\displaystyle\int_0^{\infty} F_n^{(k)}(z_j)\sin(z_j t)\,dz_j, & n \text{ odd.} \end{cases} \quad [3.15]$$

The analytical technique for evaluating the eight integrals in [3.15] is detailed in the appendix, along with the resulting closed forms of the $G_{nj}^{(k)}(t)$ functions, [A.10].

Equations [3.13] and [3.14] are solved simultaneously for $A(t)$ and $B(t)$. These functions are then substituted into the general solution, [3.6], resulting in a new expression for the stream function, [3.16] below. This new solution for $\psi$ satisfies the boundary conditions on the cylinder wall for arbitrary symmetric disturbances emanating from the spheres. Presented below is the result for $\psi$ and the velocities $v_z$ and $v_R$:

$$\psi = V\beta^2\left[\frac{1}{2}\left(\frac{R}{\beta}\right)^2 - \frac{1}{4}\left(\frac{R}{\beta}\right)^4\right] + \sum_j \sum_{n=2}^{\infty} [C_{nj}S_{nj}^{(1)}(R, z) + D_{nj}T_{nj}^{(1)}(R, z)], \quad [3.16]$$

$$v_z = V\left(1 - \frac{R^2}{\beta^2}\right) + \sum_j \sum_{n=2}^{\infty} [C_{nj}S_{nj}^{(2)}(R, z) + D_{nj}T_{nj}^{(2)}(R, z)], \quad [3.17]$$

$$v_R = \sum_j \sum_{n=2}^{\infty} [C_{nj}S_{nj}^{(3)}(R, z) + D_{nj}T_{nj}^{(3)}(R, z)], \quad [3.18]$$

where the $S_{nj}^{(k)}(R, z)$ and $T_{nj}^{(k)}(R, z)$ are defined as follows:

$$S_{nj}^{(1)}(R, z) = r_j^{-n+1}\mathcal{T}_n(\zeta_j) + \int_0^{\infty} \xi_{nj}^{(1)}(R, t)\cos(zt)\,dt, \quad [3.19a]$$

$$T_{nj}^{(1)}(R, z) = r_j^{-n+3}\mathcal{T}_n(\zeta_j) + \int_0^{\infty} \phi_{nj}^{(1)}(R, t)\cos(zt)\,dt, \quad [3.19b]$$

$$S_{nj}^{(2)}(R, z) = r_j^{-n-1}P_n(\zeta_j) + \int_0^{\infty} \xi_{nj}^{(2)}(R, t)\cos(zt)\,dt, \quad [3.20a]$$

$$T_{nj}^{(2)}(R, z) = r_j^{-n+1}[P_n(\zeta_j) + 2\mathcal{T}_n(\zeta_j)] + \int_0^{\infty} \phi_{nj}^{(2)}(R, t)\cos(zt)\,dt, \quad [3.20b]$$

$$S_{nj}^{(3)}(R, z) = r_j^{-n-1}\frac{(n+1)\mathcal{T}_{n+1}(\zeta_j)}{\sin\theta_j} + \int_0^{\infty} \xi_{nj}^{(3)}(R, t)\sin(zt)\,dt, \quad [3.21a]$$

$$T_{nj}^{(3)}(R, z) = r_j^{-n+1}\frac{(n+1)\mathcal{T}_{n+1}(\zeta_j) - 2\zeta_j\mathcal{T}_n(\zeta_j)}{\sin\theta_j} + \int_0^{\infty} \phi_{nj}^{(3)}(R, t)\sin(zt)\,dt. \quad [3.21b]$$

The integrand envelope functions $\xi_{nj}^{(k)}(R,t)$ and $\phi_{nj}^{(k)}(R,t)$ are given by

$$\xi_{nj}^{(k)}(R,t)=\frac{1}{H(t)}[h_1^{(k)}(R,t)G_{nj}^{(3)}(t)+h_2^{(k)}(R,t)G_{nj}^{(1)}(t)],$$
$$\phi_{nj}^{(k)}(R,t)=\frac{1}{H(t)}[h_1^{(k)}(R,t)G_{nj}^{(4)}(t)+h_2^{(k)}(R,t)G_{nj}^{(2)}(t)] \quad k=1,2,3, \tag{3.22}$$

where

$$H(t)=\beta^2 tI_0(\beta t)[1-\Omega^2(\beta t)]-2\beta I_1(\beta t), \tag{3.23}$$

$$h_1^{(1)}(R,t)=[2+\beta t\Omega(\beta t)]RI_1(Rt)-R^2tI_0(Rt), \tag{3.24a}$$

$$h_2^{(1)}(R,t)=\beta\Omega(\beta t)R^2I_0(Rt)-\beta^2RI_1(Rt), \tag{3.24b}$$

$$h_1^{(2)}(R,t)=[2+\beta t\Omega(\beta t)]tI_0(Rt)-t[RtI_1(Rt)+2I_0(Rt)], \tag{3.25a}$$

$$h_2^{(2)}(r,t)=\beta\Omega(\beta t)[RtI_1(Rt)+2I_0(Rt)]-\beta^2tI_0(Rt), \tag{3.25b}$$

$$h_1^{(3)}(R,t)=\frac{t}{R}h_1^{(1)}(R,t), \tag{3.26a}$$

$$h_2^{(3)}(R,t)=\frac{t}{R}h_2^{(1)}(R,t), \tag{3.26b}$$

and

$$\Omega(\beta t)=I_1(\beta t)/I_0(\beta t). \tag{3.27}$$

The integrations indicated in [3.19], [3.20], and [3.21] must be carried out numerically.

Equation [3.16] is the solution to the governing equation, [2.4], which satisfies the boundary conditions at infinity and all along the cylinder wall, $R=\beta$, independently of the $C_{nj}$ and $D_{nj}$ unknown coefficients. These coefficients are used to enforce the appropriate conditions on the surfaces of the spheres.

*The sphere boundary conditions*

The boundary conditions on the surface of sphere $j$ are given by [2.14]: $v_z=U_j$, $v_R=0$, where $U_j$ is the velocity of the sphere relative to the tube and $v_z$ and $v_R$ are given by [3.17] and [3.18]. The technique of applying these conditions is analagous to the multipole truncation method employed by Gluckman *et al.* (1971) for the unbounded flow problem.

To satisfy the boundary conditions exactly along the entire generating arc of each sphere would require the solution of the entire infinite array of unknown coefficients. The truncation technique enforces the boundary conditions at a finite number of discrete points on each sphere's generating arc and truncates the infinite series into a finite one,

$$\psi=V\beta^2\left[\frac{1}{2}\left(\frac{R}{\beta}\right)^2-\frac{1}{4}\left(\frac{R}{\beta}\right)^4\right]+\sum_j\sum_{n=2}^{M+1}[C_{nj}S_{nj}^{(1)}(R,z)+D_{nj}T_{nj}^{(1)}(R,z)]. \tag{3.28}$$

The two unknown coefficients in each inner term of the double summation permit one to satisfy the exact no-slip boundary conditions at one discrete point on each sphere. Thus, if a spherical boundary is to be approximated by satisfying conditions [2.14] at $M$ discrete points on its generating arc, $M$ terms are retained in the inner series expansion, as in [3.28]. If there are $N$ spheres in the chain, this results in a linear set of $2MN$ simultaneous algebraic equations for the $2MN$ $C_{nj}$ and $D_{nj}$ unknown coefficients of the truncated solution:

$$\sum_j\sum_{n=2}^{M+1}[C_{nj}S_{nj}^{(2)}(R_{mk},z_{mk})+D_{nj}T_{nj}^{(2)}(R_{mk},z_{mk})]=U_k-V\left(1-\frac{R_{mk}^2}{\beta^2}\right),$$
$$\sum_j\sum_{n=2}^{M+1}[C_{nj}S_{nj}^{(3)}(R_{mk},z_{mk})+D_{nj}T_{nj}^{(3)}(R_{mk},z_{mk})]=0 \tag{3.29}$$
$$\text{at } m^{\text{th}} \text{ point on sphere } k; \quad m=1,2,\ldots,M; \quad \text{all} \quad k.$$

This matrix equation can be solved by any of the standard matrix reduction techniques.

The accuracy of the present truncation technique can be improved to any degree by taking a sufficiently large value of $M$, the order of the truncation. Naturally, as $M \to \infty$ the truncation error reduces to zero, and the overall accuracy is then limited only by the accuracy achieved in the numerical integrations which are performed in evaluating the matrix elements. As will be seen in section 5, the series converges quite rapidly, and very good accuracy is achieved with only a small number of boundary points on each sphere.

## 4. VISCOUS DRAG FORCE

The force exerted by the fluid on a spherical boundary, $r_j$ = constant, is shown by Happel & Brenner (1965) to be

$$F_j = \mu\pi \int_0^\pi r_j^3 \sin^3\theta_j \frac{\partial}{\partial r_j}\left[\frac{E^2\psi}{r_j^2 \sin^2\theta_j}\right] r_j d\theta_j. \qquad [4.1]$$

Application of this operator and the orthogonality properties of the Gegenbauer functions to [3.16] results in the simple relation

$$F_j = 4\pi\mu D_{2j}. \qquad [4.2]$$

That is, only the first order term ($n = 2$) of the inner series of [3.16] contributes to the drag force on each submerged sphere.

The classical Stokes result for the drag force on an isolated sphere of radius $\alpha = a\beta$ moving with velocity $U$ is

$$F = 6\pi\mu\alpha U. \qquad [4.3]$$

On the other hand, the drag in the presence of other solid boundaries is commonly expressed in terms of a convenient drag correction factor, $\lambda$. Two drag correction factors are defined: $\lambda^{(U)}$ for spheres moving through a stationary fluid, and $\lambda^{(V)}$ for stationary spheres in a fluid whose far-downstream velocity is given by [2.12].

For spheres moving with velocities $U_j$ through an otherwise quiescent fluid ($V = 0$), we have, for sphere $j$,

$$F_j = 4\pi\mu D_{2j}^{(U)} = 6\pi\mu\alpha U_j \lambda_j^{(U)}, \qquad [4.4]$$

and hence

$$\lambda_j^{(U)} = \frac{D_{2j}^{(U)}}{1.5\alpha U_j}. \qquad [4.5]$$

That is, $\lambda_j^{(U)}$ is the ratio of the drag force on sphere $j$ to that on an isolated sphere moving with velocity $U_j$ through a quiescent fluid.

On the other hand, in the case of flow past stationary spheres ($U_j = 0$, all $j$), we have

$$F_j = 4\pi\mu D_{2j}^{(V)} = -6\pi\mu\alpha V \lambda_j^{(V)}, \qquad [4.6]$$

and hence

$$\lambda_j^{(V)} = -\frac{D_{2j}^{(V)}}{1.5\alpha V}. \qquad [4.7]$$

Here, too, $\lambda_j^{(V)}$ is seen as the ratio of $F_j$ to the drag force on a single stationary sphere in an infinite fluid of uniform velocity $V$. The negative sign arises from the fact that the $D_{2j}^{(V)}$ are necessarily negative.

When both the fluid and spheres are moving, the linearity of the equation of motion suggests that the net drag is the algebraic sum of the two drag forces discussed above, i.e.

$$F_j = 4\pi\mu D_{2j} = 4\pi\mu [D_{2j}^{(U)} + D_{2j}^{(V)}], \tag{4.8}$$

and

$$F_j = 6\pi\mu\alpha [U_j\lambda_j^{(U)} - V\lambda_j^{(V)}]. \tag{4.9}$$

It is thus necessary to consider only cases in which $U_j = 0$ (all $j$) or $V = 0$ and to treat the problem of the simultaneous motion of fluid and spheres as a superposition of its component problems.

Examination of [3.29], [4.5] and [4.7] reveals that $\lambda_j^{(U)}$ and $\lambda_j^{(V)}$ are strongly dependent on the system geometry, but that $\lambda_j^{(V)}$ is independent of $V$ for all $j$. On the other hand, $\lambda_j^{(U)}$ is a function of all $N$ sphere velocities.

A number of possible applications of [4.9] come to mind. One problem of interest considers one or two spheres suspended in a vertical tube in which fluid is being pumped against gravity. The flowrate required to keep the spheres stationary in the gravitational field is sought. Setting $U_j = 0$ and equating $F_j$ to the force of gravity, one finds from [4.9] that

$$V = \frac{U_t}{\lambda^{(V)}}, \tag{4.10}$$

where $U_t$ is the infinite-medium, isolated-sphere, terminal settling velocity, $U_t = 2\alpha^2(\rho_{\text{sphere}} - \rho)g/9\mu$.

Another application, of significant practical interest, is the zero-drag motion of spheres in a Poiseuille flow. When the particles are free to move along with the fluid and there are no body forces present in the direction of motion, they will tend to travel with different velocities such that the net drag force on each sphere is zero. Equation [4.9] indicates that this requires the fluid resistance to the motion of a sphere to exactly cancel the convective pull of the moving fluid, for each sphere of the chain. Although these zero-drag sphere velocities can be calculated from [4.9],

$$\frac{U_j}{V} = \frac{\lambda_i^{(V)}}{\lambda_j^{(U)}}, \quad \text{all} \quad j, \tag{4.11}$$

their solution in this manner is cumbersome, since [4.11] is a set of nonlinear simultaneous equations for the velocities $U_j$, each $\lambda_j^{(U)}$ being a function of all the sphere velocities.

A simpler, more direct approach is available. In solving the linear set [3.29], the $N$ $D_{2j}$ coefficients are set to zero, and replaced by the $N$ $U_k$ velocity terms by transposition of terms. The number of equations and unknowns thus preserved, the matrix equation is then solved for the sphere velocities along with the rest of the $C_{nj}$ and $D_{nj}$ coefficients.

A third application is the calculation of wall correction factors to experimental data. In general, experimental information about particle dynamics in an infinite medium is obtained by dropping spheres in a large vessel and measuring their terminal settling velocities. To correct the experimentally measured velocities for the influence of the unavoidably finite cylindrical boundary, the factors $k_{\text{I}}$ and $k_{\text{II}}$ are defined, [e.g. see Happel & Pfeffer (1960)] so that

$$\lambda_\infty = \frac{k_{\text{I}}U_{\text{I}}}{k_{\text{II}}U_{\text{II}}}. \tag{4.12}$$

Here $k_{\text{I}}$ and $k_{\text{II}}$ are wall correction factors for one and two spheres, accounting solely for the influence of the tube wall; $\lambda_\infty$ is the particle interaction parameter for an infinite medium, accounting solely for inter-particle interaction effects; $U_{\text{I}}$ and $U_{\text{II}}$ are the experimentally observed one-sphere and two-sphere terminal settling velocities.

The wall–sphere interactions are thus effectively separated from the sphere–sphere interaction effects, giving wall interaction parameters which can be used to correct experimental data. If $\lambda$ is the overall drag correction factor, defined by [4.4] or [4.6] accounting for both wall and inter-particle interactions, it is easily seen that [4.12] reduces to

$$\lambda = \lambda_\infty k_{II}. \qquad [4.13]$$

Equation [4.13] will be used to calculate the wall correction factors for two spheres, $k_{II}$, and also for three spheres, $k_{III}$.

## 5. SOLUTIONS FOR ONE SPHERE

Solutions, using the truncation technique, for the creeping flow past a single concentric sphere inside a long cylindrical tube will be presented in this section. The results of Haberman & Sayre (1958) will provide a convenient comparison.

The most accurate lowest order truncation solution for the viscous drag force is obtained by choosing one point at $\theta_j = \pi/2$ on the sphere's semi-circular generating arc for satisfying the no-slip boundary conditions. This point is the most advantageous since it controls the projected area as well as the sphere-to-cylinder diameter ratio of the boundary shape approximating the sphere. Additional points are selected as mirror-image pairs about the line $\theta_j = \pi/2$ in order to preserve the geometric symmetry of the spherical boundary shape about this line. The procedure used in the present analysis for spacing these points along each boundary was to divide the half arc of the sphere into equal segments.

An examination of the system [3.29] shows that when the $\theta_j = \pi/2$ point is used the equations become linearly dependent. In order to overcome this difficulty, the top point can be considered to be a doublet of closely adjacent points, i.e. $\theta_j = \pi/2 \pm \delta$. The optimum value of $\delta$ is found by considering a succession of one sphere solutions in which the boundary conditions are satisfied at the top doublet point only, and varying $\delta$. Examination of table 1 reveals that both $\lambda^{(U)}$ and $\lambda^{(V)}$ converge to five significant figures for all sphere-to-cylinder diameter ratios, **a**, when $\delta \leq 0.8°$. Consequently, $\delta$ was taken as 0.8° in all problems treated in this study, and these two top points at $\theta_j = 89.2°$ and $\theta_j = 90.8°$ were considered to be the single high point required.

The fundamental issue of series convergence rate still begs resolution. We must resolve the question of what order truncation solution is necessary, or at how many points on each sphere should the boundary conditions be satisfied, in order to achieve results of prescribed accuracy. The discrete point representation used in this study describes a distorted boundary shape which leads to truncation errors in the calculated drag force and velocity field. However, since the diameter ratio, **a**, and the projected area normal to the flow direction are the same for the distorted boundary as for a perfect sphere, the drag force on small, widely spaced spheres is not expected to be greatly affected by the number of boundary points used. However, in the case of large or closely spaced spheres, the exact boundary shape plays an increasing role in the sphere–cylinder interaction or the inter-particle shielding, and consequently the solution is expected to converge more slowly.

Table 1. Drag factors for one sphere, $M = 1$. Convergence tests for optimum $\delta$

| | Diameter ratio, $a = 0.1$ | | $a = 0.4$ | | $a = 0.6$ | |
|---|---|---|---|---|---|---|
| $\delta$ | $\lambda^{(U)}$ | $\lambda^{(V)}$ | $\lambda^{(U)}$ | $\lambda^{(V)}$ | $\lambda^{(U)}$ | $\lambda^{(V)}$ |
| 5° | 1.2630 | 1.2499 | 3.7811 | 3.1302 | 24.127 | 14.277 |
| 3° | 1.2638 | 1.2507 | 3.8352 | 3.1917 | 25.251 | 15.709 |
| 2° | 1.2640 | 1.2513 | 3.8770 | 3.2380 | 25.862 | 16.510 |
| 1° | 1.2641 | 1.2514 | 3.8895 | 3.2688 | 26.489 | 16.956 |
| 0.9° | 1.2641 | 1.2515 | 3.8902 | 3.2677 | 26.491 | 16.957 |
| 0.8° | 1.2641 | 1.2515 | 3.8905 | 3.2682 | 26.493 | 16.958 |
| 0.7° | 1.2641 | 1.2515 | 3.8905 | 3.2682 | 26.493 | 16.958 |

To obtain more precise information, the convergence characteristics of the one and two sphere problems were examined over a range of diameter ratios and spacings. Table 2 shows the drag correction factors, $\lambda^{(U)}$ and $\lambda^{(V)}$, for a single sphere at various $M$ and $\mathbf{a}$. The table reveals a rapid convergence which is in dramatic contrast to the behavior of the method of reflections. Convergence to four significant figures is obtained when the boundary conditions are satisfied at a surprisingly small number of points on the sphere's generating arc. Even at $\mathbf{a} = 0.8$ only fifteen points are required, and the convergence is remarkably fast at the lower diameter ratios—five points at $\mathbf{a} = 0.3$, three points at $\mathbf{a} = 0.1$. (As $\mathbf{a} \to 0$, [3.28] with $M = 1$ reduces to the exact isolated sphere Stokes solution.) The truncation error ranges from 0.022% at $\mathbf{a} = 0.3$ to 14.6% at $\mathbf{a} = 0.7$ when only three points on the generating arc are used.

Haberman & Sayre (1958) obtained the solution for a single sphere moving along the axis of an infinite cylinder. Table 3 compares their solutions and the infinite chain results of Wang & Skalak (1969) with the drag correction factors obtained by the present truncation method. The Haberman & Sayre results and the present solutions agree to within 0.5% for diameter ratios of up to 0.6, but differ somewhat as the sphere radius approaches that of the tube. The results of the present theory listed in table 3 appear to be converged solutions, in the sense that further increases in the order of truncation result in no apparent improvement. Since Haberman & Sayre do not address the topic of convergence, a question arises concerning the complete convergence of their solutions. These doubts stem from the observation that Haberman & Sayre's results consistently fall between those of the present theory and their first-order truncation approximate solution.

Table 2. Convergence of one-sphere solutions at various diameter ratios

| Diameter ratio, $\mathbf{a}$ | Number of points, $M$ | $\lambda^{(U)}$ | $\lambda^{(V)}$ |
|---|---|---|---|
| 0.1 | 1 | 1.264 | 1.252 |
| | 3 | 1.263 | 1.255 |
| | 5 | 1.263 | 1.255 |
| 0.3 | 1 | 2.429 | 2.211 |
| | 3 | 2.372 | 2.231 |
| | 5 | 2.373 | 2.231 |
| | 7 | 2.373 | 2.231 |
| 0.5 | 1 | 7.575 | 5.682 |
| | 3 | 5.936 | 4.989 |
| | 5 | 5.975 | 5.018 |
| | 7 | 5.973 | 5.017 |
| | 9 | 5.973 | 5.017 |
| 0.7 | 1 | −38.73 | −19.76 |
| | 3 | 21.60 | 15.66 |
| | 5 | 25.59 | 18.08 |
| | 7 | 25.26 | 17.89 |
| | 9 | 25.30 | 17.91 |
| | 11 | 25.29 | 17.91 |
| | 13 | 25.29 | 17.91 |

Table 3. Comparison of one-sphere solutions with results of Haberman & Sayre (1958). Wang & Skalak solutions are for an infinite chain of spheres which are 40 cylinder radii apart

| | | | Haberman & Sayre | | Wang & Skalak | |
|---|---|---|---|---|---|---|
| $a$ | $\lambda^{(U)}$ | $\lambda^{(V)}$ | $\lambda^{(U)}$ | $\lambda^{(V)}$ | $\lambda^{(U)}$ | $\lambda^{(V)}$ |
| 0.0 | 1.000 | 1.000 | | | | |
| 0.1 | 1.263 | 1.255 | 1.263 | 1.255 | 1.263 | 1.255 |
| 0.2 | 1.680 | 1.636 | 1.680 | 1.635 | 1.680 | 1.635 |
| 0.3 | 2.373 | 2.231 | 2.371 | 2.231 | 2.370 | 2.229 |
| 0.4 | 3.599 | 3.223 | 3.596 | 3.218 | 3.592 | 3.216 |
| 0.5 | 5.973 | 5.017 | 5.970 | 5.004 | 5.949 | 4.996 |
| 0.6 | 11.20 | 8.696 | 11.14 | 8.651 | 11.10 | 8.617 |
| 0.7 | 25.29 | 17.19 | 24.96 | 17.67 | 24.70 | 17.49 |

On the other hand, the Wang & Skalak (1969) drag solutions for an infinite chain of spheres seem to lend support to the Haberman & Sayre results by approaching them as the inter-sphere spacing grows large. Although the largest spacing presented by Wang & Skalak is 40 tube radii, which, in view of the slow decay properties of Stokes flow disturbances, is by no means infinite, a discrepancy may exist in the present solution technique as $\mathbf{a} \to 1.0$. This error would be due to the distortion of the spherical boundary shape resulting from the discrete rather than continuous application of boundary conditions on the sphere surface. As $M$ increases, the distorted shape converges to true sphericity, but may do so very slowly if the boundary points are selected with equal spacing on the generating arc of the spheres. The effect of this distortion on the sphere-wall interaction, however, is significant only at large diameter ratios.

In view of the above discussion, a further look into the problem for $\mathbf{a} \geq 0.7$ may be warranted. For example, a possible study would examine the convergence of the present solution with increasing $M$, when the $M$ boundary points are concentrated near the top of the sphere, thus effecting a local correction of the distortion near the tube wall. This may yield results which are in closer agreement with Haberman & Sayre's solutions for values of $\mathbf{a} \geq 0.7$. A closely related problem, the selection of boundary points for the near collision approach of two spheres, is described in Leichtberg *et al.* (1976*a*).

## 6. SOLUTIONS FOR MULTIPLE SPHERES

This section will examine the solutions for flow in a tube past finite chains of two or more spheres. To the best of the authors' knowledge exact solutions to this problem do not exist in the literature.

In order to examine the solutions' rate of convergence as a function of particle spacing, a number of solutions to the two sphere problem at various diameter ratios and sphere spacings are presented in table 4. This study reveals a slower convergence than was exhibited for the single sphere, since the intersphere interaction is adversely affected by the boundary shape distortions resulting from using a finite number of points $M$. However, the solution still converges quite rapidly, particularly at the greater spacing. In the most difficult case of spheres touching ($d/2a = 1$), the minimum number of points required for a solution which is accurate to four significant figures ranges from seven at $\mathbf{a} = 0.1$ to fifteen at $\mathbf{a} = 0.7$ (and also at $\mathbf{a} = 0.8$).

Table 5 demonstrates the proper asymptotic approach of the drag results as $\mathbf{a} \to 0$ to the values predicted by the unbounded flow theory of Stokes (1851) for one sphere, of Stimson & Jeffery (1926) for two spheres, and of Gluckman *et al.* (1971) for three spheres.

Since solution of the flow past $N$ spheres with $M$ boundary-condition points on each generating arc involves the reduction of a $2MN$ by $2MN$ matrix equation, in which each element

Table 4. Convergence of two-sphere solutions at various diameter ratios, for sphere spacings $d/2a = 1$ (touching) and $d/2a = 2$

| Diameter ratio, $a$ | Number of points $M$ | $d/2a = 1$ $\lambda^{(U)}$ | $d/2a = 1$ $\lambda^{(V)}$ | $d/2a = 2$ $\lambda^{(U)}$ | $d/2a = 2$ $\lambda^{(V)}$ |
|---|---|---|---|---|---|
| 0.1 | 3 | 0.9306 | 0.88 80 | 1.078 | 1.006 |
| | 5 | 0.9321 | 0.8899 | 1.077 | 1.005 |
| | 7 | 0.9328 | 0.8907 | 1.077 | 1.005 |
| | 9 | 0.9328 | 0.8907 | 1.077 | 1.005 |
| 0.3 | 5 | 2.072 | 1.917 | 2.320 | 2.117 |
| | 7 | 2.076 | 1.920 | 2.320 | 2.117 |
| | 9 | 2.076 | 1.920 | 2.320 | 2.117 |
| 0.5 | 7 | 5.654 | 4.913 | 5.968 | 4.987 |
| | 9 | 5.655 | 4.909 | 5.968 | 4.988 |
| | 11 | 5.656 | 5.911 | 5.968 | 4.988 |
| | 13 | 5.656 | 5.911 | 5.968 | 4.988 |
| 0.7 | 11 | 24.39 | 17.47 | 25.28 | 17.50 |
| | 13 | 24.42 | 17.46 | 25.28 | 17.50 |
| | 15 | 24.41 | 17.46 | 25.28 | 17.50 |
| | 17 | 24.41 | 17.46 | 25.28 | 17.50 |

Table 5. Asymptotic behavior of the calculated $\lambda^{(U)}$ as $a \to 0$, for one, two, and three spheres

| | | $\lambda^{(U)}$ | | | | | | | |
|---|---|---|---|---|---|---|---|---|---|
| | | Two spheres | | | Three spheres | | | | |
| | | $d/2a = 1$ | $d/2a = 2$ | | $d/2a = 1$ | | | $d/2a = 1.5$ | |
| $a$ | One sphere | Spheres −1 & 1 | Spheres −1 & 1 | Sphere −1 | Sphere 0 | Sphere 1 | Sphere −1 | Sphere 0 | Sphere 1 |
| 0.4 | 3.599 | 3.339 | 3.583 | 3.191 | 2.753 | 3.191 | 3.409 | 3.168 | 3.409 |
| $10^{-1}$ | 1.263 | 0.9328 | 1.077 | 0.8613 | 0.5077 | 0.8613 | 0.9633 | 0.6938 | 0.9633 |
| $10^{-2}$ | 1.022 | 0.6632 | 0.7662 | 0.6196 | 0.3538 | 0.6196 | 0.6707 | 0.4611 | 0.6707 |
| $10^{-3}$ | 1.002 | 0.6469 | 0.7446 | 0.6082 | 0.3273 | 0.6082 | 0.6486 | 0.4459 | 0.6486 |
| $10^{-4}$ | 1.0002 | 0.6453 | 0.7425 | 0.6064 | 0.3263 | 0.6064 | 0.6465 | 0.4444 | 0.6465 |
| $10^{-5}$ | 1.0000 | 0.6452 | 0.7423 | 0.6062 | 0.3262 | 0.6062 | 0.6463 | 0.4443 | 0.6463 |
| 0 unbounded theory | 1.000 | 0.6452 | 0.7423 | 0.6062 | 0.3262 | 0.6062 | 0.6462 | 0.4442 | 0.6462 |

of the coefficient matrix is evaluated by a numerical integration to infinity, the computing time can become a serious practical limitation. In that respect, a substantial saving can be realized by making use of the symmetry of the solution about the $z = 0$ plane. It is easily verified that the $S_{nj}^{(k)}(R, z)$ and $T_{nj}^{(k)}(R, z)$ matrix elements obey the relation

$$\left.\begin{aligned} S_{n,-j}^{(k)}(R, -z) &= (-1)^{n+k} S_{nj}^{(k)}(R, z) \\ T_{n,-j}^{(k)}(R, -z) &= (-1)^{n+k} T_{nj}^{(k)}(R, z) \end{aligned}\right\} k = 2, 3. \qquad [6.1]$$

Therefore, only the $2M^2N^2$ matrix elements related to the boundary condition points on one side of the symmetry plane need be evaluated via numerical integration, while the other $2M^2N^2$ elements are formed from [6.1].

Solutions to flow past chains containing 1, 2, 3, 5, 7 and 9 spheres have been obtained, with the boundary conditions being satisfied at a sufficiently large number of points to achieve proper convergence to four significant figures. Actual computer execution times on the IBM 370/168 were found to be approx. $[(1/4)(M + 1)N]^2$ s per case, ranging from 3 s for one sphere with five points to 21 min for nine spheres with fifteen points per generating arc. It was, therefore, out of the realm of practicality to obtain solutions for 9 or more touching spheres which converged to four significant digits.

The drag correction factors for two-sphere chains are shown in figures 2 and 3. The one-sphere solutions and Wang & Skalak's (1969) infinite chain results are also shown for reference. Since the effect of the inter-sphere interactions is a reduction in drag force, the drag is seen to decrease with increasing chain length and narrowing interparticle gaps. The effect of the enclosing boundary, however, is a marked increase in the drag force which rises beyond bound as the lubrication limit is approached between the spheres and the tube wall. For $\mathbf{a} \to 0$, the results approach the unbounded flow values, as expected.

The values of $\lambda^{(U)}$ for $\mathbf{a} = 0.2$, $d/2a = 1$ and 2, are plotted in figure 4 for chains containing different numbers of equally spaced spheres, and are shown again in figure 5 for $\mathbf{a} = 0.5$. The infinite chain results of Wang & Skalak (1969) are also shown. Solid lines connect the discrete values to denote individual chains.

The two figures vividly demonstrate the shielding characteristics of the interparticle interactions. The drag forces appear to be strongly dependent on the spacing between the spheres and on the number of spheres in the chain. The shielding effect is similarly responsible for the rapid change in drag as the end of a chain is approached, due to the fact that the end spheres receive the least amount of interactive shielding. The behavior of these end spheres with increasing chain length is underscored by the dashed curves.

The shielding effects discussed above are very strong at $d/2a = 1$, but are reduced, or damped, drastically at $d/2a = 2$. Since this is particularly true at the higher diameter ratio, one is

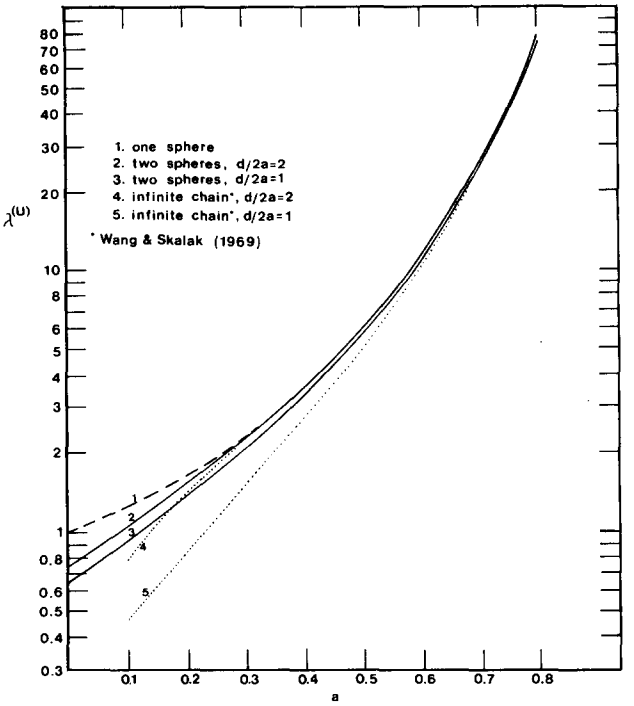


Figure 2. Drag correction factor $\lambda^{(U)}$ vs. diameter ratio.

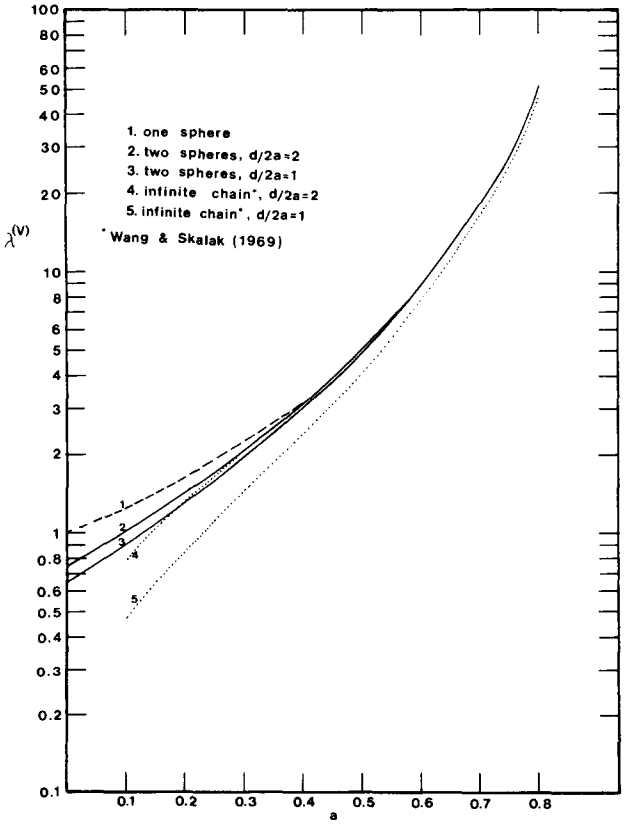


Figure 3. Drag correction factor $\lambda^{(V)}$ vs. diameter ratio.

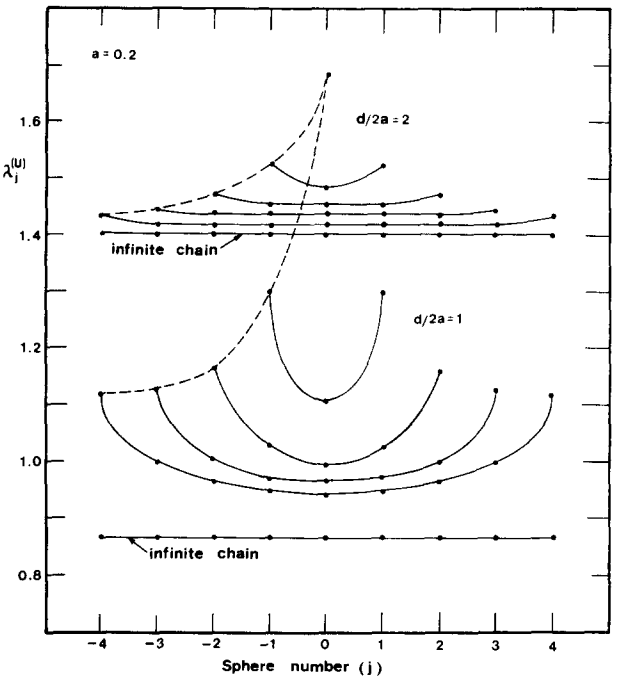


Figure 4. Drag correction factors $\lambda_j^{(U)}$ for chains containing various numbers of spheres of diameter ratio 0.2.

led to consider the damping effect which the tube wall has on the interaction forces. This wall damping is clearly illustrated when one considers, for example, the four three-sphere curves in figures 4 and 5. The striking feature to be noted is that the degree of interparticle interaction, or shielding, as measured for each chain by the curvature of its drag curve and by its departure from the drag force calculated for a single sphere, is more strongly affected by changes in the spacing

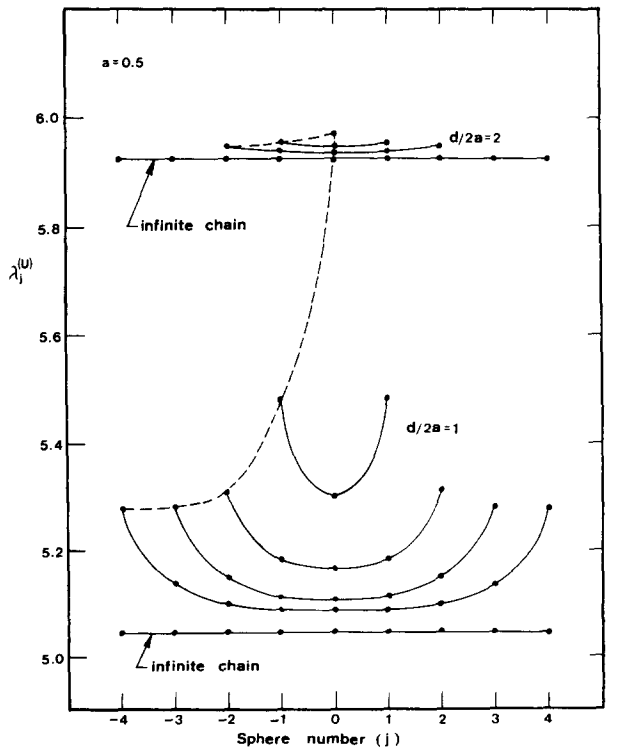


Figure 5. Drag correction factors $\lambda_j^{(U)}$ for chains containing various numbers of spheres of diameter ratio 0.5.

at the higher diameter ratio. Thus, while the diameter ratio has a moderate effect on the degree of shielding within closely packed chains, it appears to have a strong damping effect as the chain dilutes.

A sphere executing zero-drag motion in a Poiseuille flow must, if energy dissipation is to be minimized, travel with a velocity which is less than the undisturbed centerline velocity, $V/2 < U_j < V$.† The disturbed velocity profiles due to such a sphere are marked by a local reduction in the centerline velocity. Consequently, when other spheres are present in the flow field, the interactions are characterized by the transmission of this centerline velocity defect due to each sphere to the boundaries of all the other spheres. Hence, the effect of the inter-particle interaction is to decrease the sphere velocities, which is the reverse of what is observed for a chain of spheres falling under gravity in a quiescent fluid.

The values of $U/V$ for one sphere are plotted against diameter ratios in figure 6. Also shown, for reference, are the infinite chain results of Wang & Skalak (1969) for $d/2a = 1$. The third curve is the approximate results obtained in Leichtberg *et al.* (1976*b*) for a single sphere moving with zero drag along the centerline of a parabolic fluid velocity profile in an unbounded medium, i.e. in a fictitious Poiseuille flow $v = V(1 - R^2/\beta^2)$ which exists without the benefit of a solid wall at $R = \beta$. Figure 6 seems to indicate that the tube wall has no effect on the sphere's velocity for

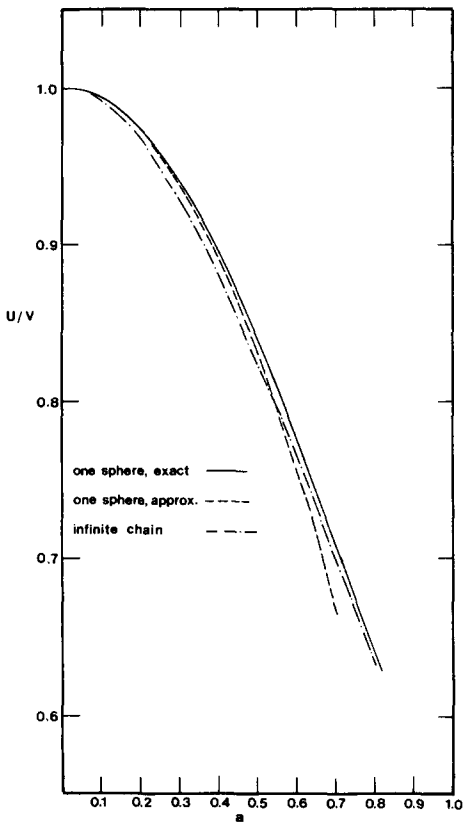


Figure 6. Zero-drag velocity vs. diameter ratio for one sphere, exact and approximate. Also shown are Wang & Shalak (1969) solutions for an infinite chain of contiguous spheres.

$a < 0.2$, and exerts only a modest influence at the higher diameter ratios. Similar behavior is observed for the motion of two spheres since the two spheres experience equal interactions. A comparison of the results for chains of three or more spheres, however, shows that the wall does exert a significant influence on the intrachain, inter-sphere interaction.

†A consequence of this constraint is $\lambda_j^{(V)} < \lambda_j^{(U)}$, witness [4.11].

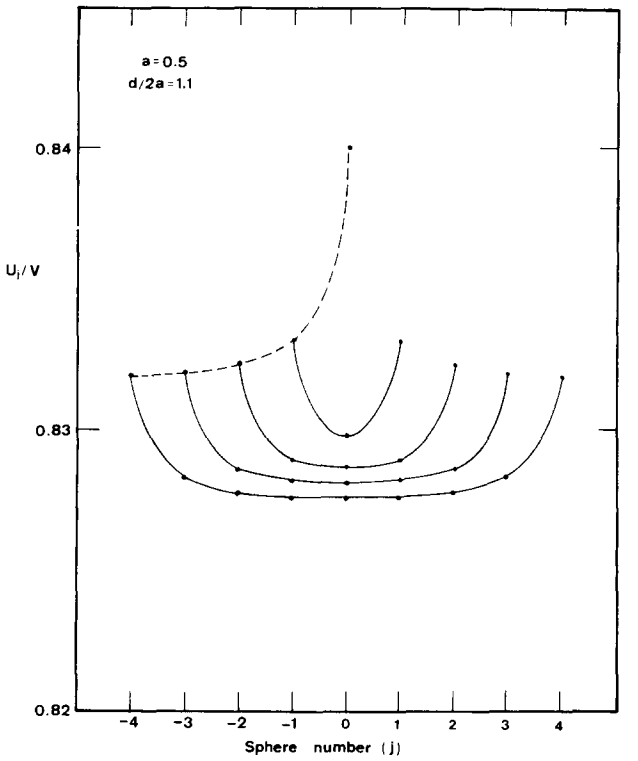


Figure 7. Zero-drag velocities in chains of diameter ratio 0.5, $d/2a = 1.1$, and varying length.

Figure 7 presents the zero-drag velocities for chains of equal spacings and various lengths, with $\mathbf{a} = 0.5$ and $d/2a = 1.1$. One observes that increasing the chain length tends to decrease the sphere velocities, and that the outer spheres of a given chain move faster than the central ones, clearly demonstrating the interactions and their end effects, respectively.

The effect of increasing the diameter ratio is a reduction in the mean Poiseuillian velocity seen by the spheres and, hence, a decrease in their zero-drag velocities relative to the mean suspension velocity. The influence of the diameter ratio on the inter-sphere relative velocities requires a somewhat closer look. In the limit of vanishing sphere size, $\mathbf{a} \to 0$, the particles move in a flow field which is uniform in its undisturbed state. Consequently, $\lambda_j^{(U)} \to \lambda_j^{(V)}$ and $U_j/V \to 1$, there being no interaction between the particles. As the diameter ratio increases, however, particle interaction effects appear, due to the non-uniform velocity profile. Further increases bring the wall interaction into play, and the wall damping effects become progressively more prominent. Thus, the degree of interparticle interactions is small for $\mathbf{a} < 0.1$, reaches a maximum in the approximate range $0.3 < \mathbf{a} < 0.4$, and is quickly damped out for $\mathbf{a} > 0.5$, particularly in chains of medium concentration, $d/2a > 2$.

Figures 8 and 9 present $U_j/V$ for chains of five equally spaced spheres at various spacings, of diameter ratios of 0.3 and 0.5, respectively. A comparison of the two figures shows that the wall damping effect is of relatively little importance to the closely-packed chains, $d/2a = 1.1$ and 1.3, but is of much greater significance to the chains with larger spacing.

The interaction effects in zero-drag motion appear to be roughly two orders of magnitude smaller than the effects of the shielding phenomenon reported earlier for constrained sphere motion.

Table 6 presents, for the sake of completeness, the zero-drag velocities of one and two-sphere chains.

Equation [4.13] was used to calculate the wall correction factors. The results are presented below in the form of correlation relations, valid only for small sphere-to-tube diameter ratios **a**.

(i) Two spheres translating in a stationary fluid. Validity limited to close spacings, $1 \leq d/2a \leq 2$.

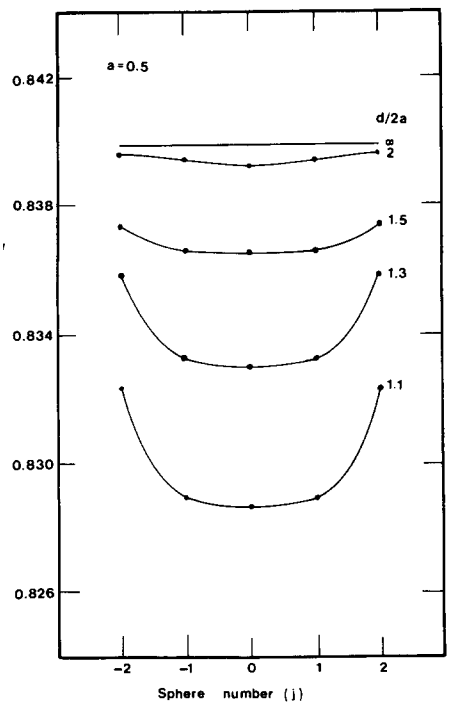


Fig. 8.

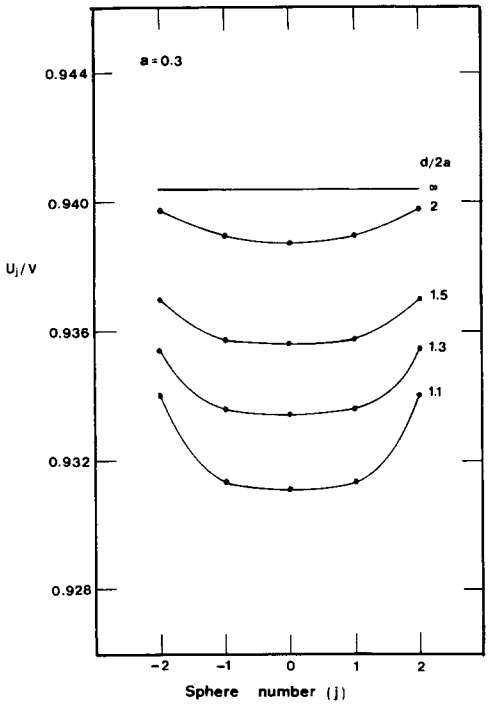


Fig. 9.

Figure 8. Zero-drag velocities in five-sphere chains of diameter ratio 0.3 and varying sphere spacings.

Figure 9. Zero-drag velocities in five-sphere chains of diameter ratio 0.5 and varying sphere spacings.

Table 6. Zero-drag velocities, $U/V$, for one and two sphere chains

| $a$ | 1 sphere | 2 spheres $d/2a = 1$ | 2 spheres $d/2a = 2$ |
|---|---|---|---|
| 0.0 | 1.000 | 1.000 | 1.000 |
| 0.1 | 0.9935 | 0.9926 | 0.9932 |
| 0.2 | 0.9734 | 0.9705 | 0.9727 |
| 0.3 | 0.9404 | 0.9378 | 0.9400 |
| 0.4 | 0.8957 | 0.8882 | 0.8953 |
| 0.5 | 0.8400 | 0.8329 | 0.8397 |
| 0.6 | 0.7763 | 0.7713 | 0.7761 |
| 0.7 | 0.7081 | 0.7042 | 0.7080 |
| 0.8 | 0.6378 | 0.6369 | 0.6378 |

ror of 0.2% at $\mathbf{a} = 0.1$, 1.4% at $\mathbf{a} = 0.2$.

$$k_{\mathrm{II}}^{(U)} = \exp\left[a(3.6591 + 0.4594a)\right]. \qquad [6.2]$$

(ii) Two spheres translating in a stationary fluid. Valid at all spacings, $1 \leq d/2a < \infty$. aximum error of 0.5% for $\mathbf{a} \leq 0.2$.

$$k_{\mathrm{II}}^{(U)} = 1 + 1.86a + 7.7a^2 + 5.552a\left(\frac{2a}{d}\right) + 1.39a^2\left(\frac{2a}{d}\right) - 4.228a\left(\frac{2a}{d}\right)^2 + 3.66a^2\left(\frac{2a}{d}\right)^2. \qquad [6.3]$$

(iii) Two stationary spheres in a Poiseuille flow. Validity limited to close spacings $1 \leq d/2a \leq 2$. ror of 1% at $\mathbf{a} = 0.1$, 2% at $\mathbf{a} = 0.2$.

$$k_{\mathrm{II}}^{(V)} = \exp\left[a(2.8376 + 2.9043a)\right]. \qquad [6.4]$$

(iv) Two stationary spheres in a Poiseuille flow. Valid at all spacings, $1 \leq d/2a < \infty$. Maximum error of 0.7% for $\mathbf{a} \leq 0.2$.

$$k_{II}^{(V)} = 1 + 1.92a + 6.3a^2 + 1.1925a\left(\frac{2a}{d}\right) + 15.115a^2\left(\frac{2a}{d}\right) - 0.599a\left(\frac{2a}{d}\right)^2 - 8.49a^2\left(\frac{2a}{d}\right)^2. \quad [6.5]$$

(v) Three spheres translating in a quiescent fluid. Validity limited to close spacings $1 \leq d/2a \leq 2$. Maximum error for $\mathbf{a} \leq 0.2$ is 5.0% for [6.6] and 2.3% for [6.7].

$$k_{III}^{(U)} = \exp\left[a(3.7051 = 0.5089a)\right], \quad \text{end spheres,} \quad [6.6]$$

$$k_{III}^{(U)} = \exp\left[a(2.7745 + 16.675a)\right], \quad \text{inner sphere.} \quad [6.7]$$

Equations [6.2], [6.4], [6.6] and [6.7] are of the form: $k = \exp\left[a(C_0 + C_1 a)\right]$, where $C_0$ and $C_1$ are arbitrary constants. This form was chosen because of the near linearity of $\ln \lambda(a)$ at small diameter ratios, as evidenced in figures 2 and 3. The coefficients $C_0$ and $C_1$ were determined by fitting the above equation to the data at $\mathbf{a} = 0.0, 0.1, 0.2$. Equations [6.3] and [6.5] were derived by fitting the form

$$k(a) = C_0(a) + C_1(a)\left(\frac{2a}{d}\right) + C_2(a)\left(\frac{2a}{d}\right)^2,$$

$$C_i(a) = P_i + q_i a + r_i a^2, \quad i = 0, 1, 2,$$

(where $p_0 = 1$, $p_1 = p_2 = 0$ to satisfy the asymptotic condition $k(0) = 1$) to the data for $2a/d = 0.0$, 0.5, 1.0 and $\mathbf{a} = 0.0, 0.1, 0.2$. The accuracy of [6.2] to [6.7] was checked at the test data points as well as at intermediate values.

*Acknowledgement*—This research was supported by National Science Foundation Grant No. GK-40802. This research was submitted by S. Leichtberg in partial fulfillment of the requirements of the Ph.D. degree from the School of Engineering of The City College of The City University of New York.

## REFERENCES

ABRAMOWITZ, M. & STEGUN, I. 1965 *Handbook of Mathematical Functions*, p. 376. Dover.

BART, E. 1959 Interaction of two spheres falling slowly in a viscous medium. M.Ch.E. Thesis, New York University.

BOHLIN, T. 1960 On the drag of a rigid sphere moving in a viscous liquid inside a cylindrical tube. *K. tek. Högsk. Handl.* No. 155.

BRENNER, H. 1970 Pressure drop due to the motion of neutrally buoyant particles in duct flows. *J. Fluid Mech.* **43**, 641–660.

BRENNER, H. 1971 Pressure drop due to the motion of neutrally buoyant particles in duct flows. II Spherical droplets and bubbles. *I/EC Fundamentals* **10**, 537–543.

BUNGAY, P. M. & BRENNER, H. 1973*a* Pressure drop due to the motion of a sphere near the wall bounding a Poiseuille flow, *J. Fluid Mech.* **60**, 81–96.

BUNGAY, P. M. & BRENNER, H. 1973*b* The motion of a closely-fitting sphere in a fluid-filled tube. *Int. J. Multiphase Flow* **1**, 25–56.

BURGERS, J. M. 1938 *Second Report on Viscosity and Plasticity*, Chapt. 3. North Holland, Amsterdam.

BURGERS, J. M. 1940 *Proc. K. ned. Akad. Wet.* **43**, 425, 646.

BURGERS, J. M. 1941 *Proc. K. ned. Akad. Wet.* **44**, 1045.

BURGERS, J. M. 1942 *Proc. K. ned. Akad. Wet.* **45**, 9.

CHEN, T. C. & SKALAK, R. 1970 Stokes flow in a cylindrical tube containing a line of spheriodal particles. *Appl. Scient. Res.* **22**, 403–441.

FAXEN, H. 1922 Die Geschwindigkeit zwen Kugeln, die unter Ein winkung der Schwere in einen zahen Flussigkeit fallen. *Ann. Phys.* **68**, 89.

FAXEN, H. 1923 Die Bewegung einer starren Kugel längs der Achse eines mit zäher Flussigkeit gefüllten Rohres. *Ark. Mat. Astr. Fys.* **17**, 1–28.

GLUCKMAN, M. J., PFEFFER, R. & WEINBAUM, S. 1971 A new technique for treating multiparticle slow viscous flow: axisymmetric flow past spheres and speroids. *J. Fluid Mech.* **50**, 705–740.

GLUCKMAN, M. J. WEINBAUM, S. & PFEFFER, R. 1972 Axisymmetric slow viscous flow past an arbitrary convex body of revolution. *J. Fluid Mech.* **55**, 677–709.

GREENSTEIN, T. & HAPPEL, J. 1970 The slow motion of two particles symmetrically placed about the axis of a circular cylinder in a direction perpendicular to their line of centers. *Appl. Scient. Res.* **22**, 345–359.

HABERMAN, W. L. & SAYRE, R. M. 1958 *Motion of rigid and fluid spheres in stationary and moving liquids inside cylindrical tubes.* David W. Taylor Model Basin Report No. 1143, U.S. Navy Dept.

HAPPEL, J. & BRENNER, H. 1965 Low Reynolds Number Hydrodynamics, p. 115. Prentice-Hall, New York.

HAPPEL, J. & BYRNE, B. J. 1954 Motion of a sphere and fluid in a cylindrical tube. *Ind. Engng Chem.* **46**, 1181–1186; corrections 1957 *Ind. Engng Chem.* **49**, 1029.

HAPPEL, J. & PFEFFER, R. 1960 The motion of two spheres following each other in a viscous fluid. *A.I.Ch.E. Jl.* **6**, 129–133.

HOCHMUTH, R. M. & SUTERA, S. P. 1970 Spherical caps in low Reynolds number tube flow. *Chem. Engng Sci.* **25**, 593–604.

HOCKING, L. M. 1964 The behavior of clusters of spheres falling in a viscous fluid. *J. Fluid. Mech* **20**, 129–139.

KYNCH, G. J. 1959 The slow motion of two or more spheres through a viscous fluid. *J. Fluid Mech.* 193–208.

LADENBURG, R. 1907 Über den Einfluss von Wanden Auf die Bewegung einer Kugel in einer reibenden Flussigkeit. *Ann. Phys.* **23**, 447–458.

LEICHTBERG, S., WEINBAUM, S., PFEFFER, R. & GLUCKMAN, M. J. 1976*a* A study of unsteady forces at low Reynolds number: a strong interaction theory for the coaxial settling of three or more spheres. *Phil. Trans. R. Soc. A.* **282**, 585–613.

LEICHTBERG, S., WEINBAUM, S. & PFEFFER, R. 1976*b* A theory for the coaxial slow viscous motion of finite clusters of spheres in unbounded Poiseuille flow and its application to rouleaux formation. *Biorheology.* **13**, 165–179.

PAYNE, L. E. & PELL, W. H. 1960 The Stokes flow problem for a class of axially symmetric bodies, *J. Fluid Mech.* **7**, 529–549.

SAMPSON, R. A. 1891 On Stokes' current-function. *Phil. Trans. R. Soc.* **A182**, 449.

SAVIC, P. 1953 Circulation and distortion of liquid drops falling through a viscous medium. *Nat. Res. Counc. Canada Rep.* No. MT-22.

SKALAK, R., CHEN, P. H. & CHIEN, S. 1972 Effect of hematocrit and rouleaux on apparent viscosity in capillaries. *Biorheology* **9**, 67–89.

SMOLUCHOWSKI, M. 1911 On the mutual action of spheres which move in a viscous liquid. *Bull. Acad. Sci. Cracow* **1A**, 28–39.

SMOLUCHOWSKI, M. 1912 On the practical applicability of Stokes law of resistance, and the modifications of it required in certain cases. *Proc. Fifth Int. Cong. Math.* **2**, 192–201.

STIMSON, M. & JEFFERY, G. B. 1926 The motion of two-spheres in a viscous fluid. *Proc. R. Soc.* **A111**, 110–116.

STOKES, G. G. 1851 On the effect of the internal friction of fluids on the motion of pendulums. *Trans. Cambr. Phil. Soc.* **9**, 8.

WAKIYA, S. 1953 A spherical obstacle in the flow of a viscous fluid through a tube. *J. Phys. Soc. Japan* **8**, 254–257.

WANG, H. & SKALAK, R. 1969 Viscous flow in a cylindrical tube containing a line of spherical particles. *J. Fluid Mech.* **38**, 75–96.

## APPENDIX

The analytical integration procedures required for the closed-form evaluation of the $G_{nj}^{(k)}(t)$ functions, [3.15], are presented here. The $F_n^{(k)}(z_j)$ functions are listed in [3.12a–d].

The eight integrals are evaluated by inductive reasoning, using the properties of the Legendre and Gebenbauer functions. We begin with the Fourier integral representation of the modified Bessel function of the second kind (see Abramowitz & Stegun, 1965).

$$K_i(t) = \pi^{-1/2}\left(\frac{2}{t}\right)^i \Gamma\left(i+\frac{1}{2}\right)\int_0^\infty (1+x^2)^{-i-(1/2)}\cos(xt)\,dx. \qquad [A.1]$$

Equation [A.1] can be manipulated and solved for the Fourier transform,

$$\frac{2}{\pi}\int_0^\infty t^i K_i(\beta t)\cos(xt)\,dt = \pi^{-(1/2)}(2\beta)^i\Gamma\left(i+\frac{1}{2}\right)(\beta^2+x^2)^{-i-(1/2)}, \quad i=0,1,2,\ldots. \qquad [A.2]$$

We first prove that

$$\frac{2}{\pi}\int_0^\infty t^n K_0(\beta t)\cos\left[xt-(n-2)\frac{\pi}{2}\right]dt = -n!\,(\beta^2+x^2)^{-(n+1)/2}P_n\left[\frac{x}{\sqrt{(\beta^2+x^2)}}\right] \quad n\geq 0. \qquad [A.3]$$

With $i=0$, [A.2] reduces to

$$\frac{2}{\pi}\int_0^\infty K_0(\beta t)\cos(xt)\,dt = (\beta^2+x^2)^{-(1/2)} = (\beta^2+x^2)^{-(1/2)}P_0\left[\frac{x}{\sqrt{(\beta^2+x^2)}}\right].$$

Successive differentiations with respect to $x$ yield

$$-\frac{2}{\pi}\int_0^\infty tK_0(\beta t)\sin(xt)\,dt = -(\beta^2+x^2)^{-1}P_1\left[\frac{x}{\sqrt{(\beta^2+x^2)}}\right],$$

$$-\frac{2}{\pi}\int_0^\infty t^2K_0(\beta t)\cos(xt)\,dt = 2(\beta^2+x^2)^{-3/2}P_2\left[\frac{x}{\sqrt{(\beta^2+x^2)}}\right].$$

The last three equations verify [A.3] for $n=0,1,2$, respectively. We now differentiate [A.3] with respect to $x$:

$$\begin{aligned}&-\frac{2}{\pi}\int_0^\infty t^{n+1}K_0(\beta t)\sin\left[xt-(n-2)\frac{\pi}{2}\right]dt\\ &= -n!(n+1)(\beta^2+x^2)^{-(n+2)/2}\left\{n\mathcal{T}_{n+1}\left[\frac{x}{\sqrt{(\beta^2+x^2)}}\right]-\frac{x}{\sqrt{(\beta^2+x^2)}}P_n\left[\frac{x}{\sqrt{(\beta^2+x^2)}}\right]\right\}\\ &= (n+1)!(\beta^2+x^2)^{-(n+2)/2}P_{n+1}\left[\frac{x}{\sqrt{(\beta^2+x^2)}}\right],\end{aligned}$$

since $\sin[xt-(n-2)\pi/2] = \cos[xt-(n-1)\pi/2]$, this completes the inductive proof of [A.3] for all $n\geq 0$.

We next write [A.2] with $i=1$ and follow with a line of induction, which parallels the proof of [A.3], to prove the following relation (details omitted)

$$\frac{2}{\pi}\int_0^\infty t^{n-1}K_1(\beta t)\cos\left[xt-(n-2)\frac{\pi}{2}\right]dt = \frac{n!}{\beta}(\beta^2+x^2)^{-(n-1)/2}\mathcal{T}n\left[\frac{x}{\sqrt{(\beta^2+x^2)}}\right], \quad n\geq 2. \qquad [A.4]$$

What follows in deriving the desired integrals centers on [A.3] and [A.4] and involves their manipulation and re-indexing. Using the properties of the Legendre and Gegenbauer polynomials, and combining the integrals in [A.3] and [A.4], it can be shown that

$$\frac{2}{\pi}\int_0^\infty t^{n-3}[(2n-3)\beta^2tK_0(\beta t)-(n-2)(n-3)\beta K_1(\beta t)]\cos\left[xt-(n-2)\frac{\pi}{2}\right]dt = n!(\beta^2+x^2)^{-(n-3)/2}\mathcal{T}_n\left[\frac{x}{\sqrt{(\beta^2+x^2)}}\right],$$

$$n\geq 2 \qquad [A.5]$$

and

$$\frac{2}{\pi}\int_0^\infty t^{n-2}[n(n-1)K_0(\beta t)-(2n-1)\beta tK_1(\beta t)]\cos\left[xt-(n-2)\frac{\pi}{2}\right]dt = n!(\beta^2+x^2)^{-(n-1)/2}P_n\left(\frac{x}{\sqrt{(\beta^2+x^2)}}\right), \quad n\geq 2.$$

[A.6]

Equations [A.3]–[A.6] all have the following general form:

$$\frac{2}{\pi}\int_0^\infty g_n^{(k)}(t)\cos\left[xt-(n-2)\frac{\pi}{2}\right]dt = n!f_n^{(k)}(x), \quad n\geq 2, \tag{A.7}$$

where [A.3, 4, 5, 6] are represented by $k = 1, 2, 3, 4$, respectively, and $f_n(-x) = (-1)^n f_n(x)$. It is further noted that

$$\cos\left[xt-(n-2)\frac{\pi}{2}\right] = \begin{cases} -(-1)^{n/2}\cos(xt), & n = \text{even} \\ -(-1)^{(n-1)/2}\sin(xt), & n = \text{odd}. \end{cases} \tag{A.8}$$

Equations [A.7] and [A.8] are combined, and the Fourier transforms are extracted, yielding

$$\int_0^\infty f_n^{(k)}(x)\begin{Bmatrix}\cos(xt)\\ \sin(xt)\end{Bmatrix}dx = \begin{Bmatrix}-(-1)^{n/2}\\ -(-1)^{(n-1)/2}\end{Bmatrix}\frac{1}{n!}g_n^{(k)}(t), \qquad \begin{matrix}\{n=\text{even}\\ n=\text{odd}\}\end{matrix}, \quad n\geq 2, \quad k = 1,2,3,4. \tag{A.9}$$

The derivation of the required integrals is now completed by comparing [A.7] to [A.3]–[A.6], extracting the eight functions $f_n^{(k)}(x)$ and $g_n^{(k)}(t)$. A subsequent glance at [3.12] reveals that

$$\begin{aligned} F_n^{(1)}(x) &= -f_n^{(1)}(x), \\ F_n^{(2)}(x) &= f_n^{(4)}(x) + 2\beta f_n^{(2)}(x), \\ F_n^{(3)}(x) &= \beta f_n^{(2)}(x), \\ F_n^{(4)}(x) &= f_n^{(3)}(x). \end{aligned}$$

Therefore, substitution for $f_n^{(k)}(x)$ and $g_n^{(k)}(t)$ in [A.9] yields the functions $G_{nj}^{(k)}(t)$ of [3.15]:

$$\begin{aligned} G_{nj}^{(1)}(t) &= -b_{nj}(t)t^n K_0(\beta t), \\ G_{nj}^{(2)}(t) &= b_{nj}(t)t^{n-2}[n(n-1)K_0(\beta t) - (2n-3)\beta t K_1(\beta t)], \\ G_{nj}^{(3)}(t) &= b_{nj}(t)\beta t^{n-1}K_1(\beta t), \\ G_{nj}^{(4)}(t) &= b_{nj}(t)\beta t^{n-3}[(2n-3)\beta t K_0(\beta t) - (n-2)(n-3)K_1(\beta t)], \end{aligned} \tag{A.10}$$

where

$$b_{nj}(t) = \begin{cases} -(-1)^{n/2}\dfrac{2}{\pi n!}\cos(jd\beta t), & n = \text{even} \\ (-1)^{(n-1)/2}\dfrac{2}{\pi n!}\sin(jd\beta t), & n = \text{odd}. \end{cases} \tag{A.11}$$